Forward Peak Structure in Quasi-Two-Body Reactions and Long-Range Pion Exchange*

PAUL R. STEVENS†‡
Department of Physics, University of California, Los Angeles, California 90024

(Received 23 December 1969)

We find that a coherent-droplet model with long-range pion exchange successfully fits the forward peak structure of the differential cross sections for $\pi^+p\to\rho^0\Delta^{++}$, $\pi^+p\to f^0\Delta^{++}$, $\pi^-p\to\rho^0n$, $\pi^+p\to\rho^+p$, $pp\to n\Delta^{++}$, $K^-p\to K^{*0}(890)n$, and $K^-p\to K^{*-}(890)p$. For $-t'<0.02$ $(\mathrm{GeV}/c)^2$, the measured differential cross sections exhibit anomalous behaviors: spikes and dips and no structure. The different behaviors are explained mainly by the kinematic structure of pion-pole residues. In some of the reactions, the known magnitude of the pion-pole residue leads us to expect structures near $t'=0$ which require data with higher statistical precision for confirmation. In $\pi^+p\to f^0\Delta^{++}$ at 8 GeV/c, our model can explain the absence of an anomaly near $t'=0$ in terms of the large distance from the physical region to the pion pole. However, this distance decreases with increasing energy, and our model predicts structure near $t'=0$ in $\pi^+p\to f^0\Delta^{++}$ at 16 GeV/c.

I. INTRODUCTION

RECENT experiments[1–3] with high statistical precision give the shapes of the differential cross sections of a number of quasi-two-body reactions in the region $-t'<0.06$ $(\mathrm{GeV}/c)^2$ (see Figs. 2 and 3).

There is a steep rise in the $\pi^+p\to\rho^0\Delta^{++}$ data[4] for $-t'<0.03$ $(\mathrm{GeV}/c)^2$. A similar spike has been seen previously in np charge exchange[5] and in the π^+ photoproduction.[6] In these reactions, the spike for $-t<0.02$ $(\mathrm{GeV}/c)^2$ has been shown to be a consequence of pion exchange dominating large-impact-parameter collisions.[7,8]

There is, however, no spike in the $\pi^+p\to f^0\Delta^{++}$ data.[1] Furthermore, a dip is seen in the $\pi^-p\to\rho^0n$ data.[3] This variety of shapes is interesting because pion exchange is allowed in these reactions also.

In this paper we show that all the observed spikes and dips for $-t'<0.03$ $(\mathrm{GeV}/c)^2$ can be explained very simply by the effects of long-range pion exchange. By long-range pion exchange we mean the high partial waves of the pion-exchange scattering amplitudes calculated using the Feynman diagram of Fig. 1(a). Indeed, the variety of structures is explained mainly by mass, spin, and isospin effects.

Long-range pion exchange contributes only for $-t'<0.06$ $(\mathrm{GeV}/c)^2$. To include this contribution and to understand the data over a larger region of t', a model for the low partial waves is necessary. In previous work, Byers[7] has shown that the coherent-droplet model with long-range pion exchange can explain the np charge-exchange differential cross section for $0>t>-0.5$ $(\mathrm{GeV}/c)^2$. Chou[9] has proposed a modified coherent-droplet model for photoproduction, and general two-body inelastic processes. This modified droplet model with long-range pion exchange describes well the π^+ photoproduction differential cross section for $0>t>-0.8$ $(\mathrm{GeV}/c)^2$. We give a possible extension of the coherent-droplet model to quasi-two-body reactions. However, in the approximation which we use, namely, that initial- and final-state elastic scattering is the same, this model is just the original droplet model of Byers and Yang.[10]

We apply the coherent-droplet model with long-range pion exchange to the following reactions:

(A) $\pi^+p\to\rho^0\Delta^{++}$,
(B) $\pi^+p\to f^0\Delta^{++}$,
(C) $\pi^-p\to\rho^0n$,
(D) $\pi^+p\to\rho^+p$,
(E) $pp\to n\Delta^{++}$,
(F) $K^-p\to K^{*0}(890)n$,
(G) $K^-p\to K^{*-}(890)p$.

The model gives good fits to the data for $-t'\lesssim 0.3$ $(\mathrm{GeV}/c)^2$ for all these reactions.

In reactions which have large mass changes at both pion vertices, the long-range pion contribution peaks sharply at $\theta=0°$. Long-range pion exchange can account for the slope and magnitude of the spike in $\pi^+p\to\rho^0\Delta^{++}$ at 8 GeV/c. In $\pi^+p\to f^0\Delta^{++}$ at 8 GeV/c, the physical region is farther from the pion pole than in $\pi^+p\to\rho^0\Delta^{++}$ at 8 GeV/c. As a result, the long-range pion contribu-

* Supported in part by the National Science Foundation.
† Submitted to the University of California at Los Angeles in partial satisfaction of the requirements for the degree of Doctor of Philosophy in Physics.
‡ National Science Foundation Predoctoral Fellow.
[1] Aachen-Berlin-CERN Collaboration, Nucl. Phys. **B8**, 45 (1968).
[2] Aachen-Berlin-CERN Collaboration, Phys. Letters **27B**, 174 (1968).
[3] B. D. Hyams, W. Koch, D. C. Potter, J. D. Wilson, J. Von Lindern, E. Lorenz, G. Lutjens, U. Stierlin, and P. Weilhammer, Nucl. Phys. **B7**, 1 (1968).
[4] In Fig. 2(b) we normalized the small-$(-t')$ data of Ref. 2 using the data of the same authors given more recently in Ref. 1.
[5] See, e.g., R. R. Wilson, *The Nucleon-Nucleon Interaction* (Interscience, New York, 1963), Fig. 6.3. Also, G. Manning, A. G. Parham, J. D. Jafar, H. B. van der Raay, D. H. Reading, D. G. Ryan, B. D. Jones, J. Malos, and N. H. Lipman, Nuovo Cimento **41A**, 167 (1966).
[6] See, e.g., A. M. Boyarski, F. Bulos, W. Busza, R. Diebold, S. D. Echlund, G. E. Fischer, J. R. Rees, and B. Richter, Phys. Rev. Letters **20**, 300 (1968).
[7] N. Byers, Phys. Rev. **156**, 1703 (1967).
[8] N. Byers and G. H. Thomas, Phys. Rev. Letters **20**, 129 (1968).
[9] T. T. Chou, Phys. Rev. **176**, 2041 (1968).
[10] N. Byers and C. N. Yang, Phys. Rev. **142**, 976 (1966).

tion is both broader and smaller than in $\pi^+p\to\rho^0\Delta^{++}$. This long-range pion contribution is consistent with the data.

As the energy increases, however, the physical region moves closer to the pion pole. Between 8 and 16 $(\mathrm{GeV}/c)^2$ in $\pi^+p\to f^0\Delta^{++}$, the long-range pion contribution at $t'=0$ remains roughly constant, while its half-width decreases. Our model predicts in $\pi^+p\to f^0\Delta^{++}$ at 16 GeV/c a spike similar in shape to that seen in $\pi^+p\to\rho^0\Delta^{++}$ at 8 GeV/c if there is no interference between long-range pion exchange and small-impact-parameter partial-wave amplitudes. The shape and magnitude of the spike is sensitive to this interference.

The other five reactions have a mass change at only one vertex. At the other vertex the nucleon goes straight through. In these reactions the single-helicity-flip pion amplitudes dominate, causing the long-range pion contribution to dip in the forward direction and to peak near $t'=-0.015$ $(\mathrm{GeV}/c)^2$. Such structure is indicated by the data for $\pi^-p\to\rho^0n$ and is consistent with the data for $\pi^+p\to\rho^+p$, $K^-p\to K^{*0}(890)n$, and $pp\to n\Delta^{++}$.[3,1,11,12] However, this structure is not seen in $K^-p\to K^{*-}(890)p$.[11] By isospin conservation, the pion contributions to $K^-p\to K^{*-}(890)p$ are four times smaller than to $K^-p\to K^{*0}(890)n$. The large $-t'$ data indicate that the low-partial-wave contributions to $K^-p\to K^{*-}(890)p$ are larger and, indeed, swamp the pion contributions even at small $-t'$.

In Sec. II we discuss an important kinematic consideration. In Sec. III we discuss the main assumptions of our model. In Secs. IV and V we give detailed discussions of the partial-wave amplitudes in our model, while in Sec. VI we discuss the scattering amplitudes. In Sec. VII we apply our analysis to seven reactions and discuss our fits. In Sec. VIII we discuss the energy dependence of long-range pion exchange. We have included two appendices on the kinematic structure of pion helicity vertex functions. One appendix discusses the kinematic structure for particles of arbitrary mass, spin, and parity; the other gives detailed expressions for the special cases analyzed in this paper. We have also included an appendix which gives simple, approximate expressions for the long-range pion contribution to scattering amplitudes. These expressions are useful for numerical calculations.

II. IMPORTANT KINEMATIC CONSIDERATION

In this paper we discuss, at finite energies, reactions $a+b\to c+d$ where c or d or both are broad resonances. In our notation $s=(p_a+p_b)^2$ and $t=(p_a-p_c)^2$. The minimum physical value of $-t$, that is, $-t$ at $\theta=0°$, is $-t_{\min}$. At large energies,

$$t_{\min}=-(m_a^2-m_c^2)(m_b^2-m_d^2)/s-(m_a^2m_b^2-m_c^2m_d^2)\times(m_a^2-m_c^2+m_b^2-m_d^2)/s^2+O(s^{-3}). \quad (1)$$

The c.m. scattering angle is θ and the c.m. three-momenta of initial- and final-state particles are $\mathbf{p}$ and $\mathbf{p}'$, respectively. The helicities are λ_a, λ_b, λ_c, and λ_d.

When c or d are resonances, $t_{\min}$ has a range of values. Consequently, the differential cross section for small t is dominated by this kinematic effect when data are plotted against t. To eliminate this effect, the data are plotted against the variable[13]

$$t'\equiv t-t_{\min}. \quad (2)$$

The relation of t' to the c.m. scattering angle is

$$t'=-4pp'\sin^2(\tfrac{1}{2}\theta). \quad (3)$$

To simplify our discussion, we shall refer to the eikonal approximation to the partial-wave expansion. We define the impact parameter to be $b=(J+\frac{1}{2})/(pp')^{1/2}$. Then the partial-wave sums for the helicity scattering amplitudes may be approximated by

$$F_{\{\lambda\}}(s,t')=p'\int\alpha_{\{\lambda\}}(b,s)J_{\Delta\lambda}(b\sqrt{-t'})\,b\,db, \quad (4)$$

where $\{\lambda\}=\{\lambda_c,\lambda_d;\lambda_a,\lambda_b\}$ and $\Delta\lambda=\lambda_c-\lambda_d-\lambda_a+\lambda_b$.[14] Note from (4) that t' rather than t is the variable conjugate to b. This is due to the relation (3). In actual numerical calculations, partial-wave sums were used.

III. MODEL

Our model is a physical assumption for the partial-wave amplitudes $\alpha_\lambda(b,s)$ in high-energy quasi-two-body scattering. The interacting hadrons are assumed to be extended objects. We use the eikonal picture in which a ray passes through an effective matter distribution. At high energies, the bulk of the matter is confined within a disk of radius a. This radius is (roughly) determined from elastic scattering. In our model the core of radius a is surrounded by a pion cloud.

For collisions with large impact parameter, $b\gg a$, scattering is mainly due to the pion cloud. For these collisions, we use the Born approximation for pion exchange.

For collisions with small impact parameter, $b\lesssim a$, the matter distributions of the colliding hadrons overlap appreciably. Many different short-range interactions can contribute. To take into account all mechanisms that can contribute to low partial waves, we use coherent-droplet-model amplitudes.

Our model applies at such energies that the wave-

[11] Aachen-Berlin-CERN-London (I.C.) -Vienna Collaboration, Nucl. Phys. **B7**, 111 (1968); **B5**, 567 (1968).

[12] H. C. Dehne, J. Diaz, K. Stromer, A. Schmitt, W. P. Swanson, I. Borecka, G. Knies, and G. Wolf, Nuovo Cimento **53A**, 232 (1968).

[13] See, e.g., Refs. 1–3. See also J. T. Donahue, Nuovo Cimento **55A**, 527 (1968).

[14] We use the partial-wave expansion for helicity amplitudes given by M. Jacob and G. C. Wick, Ann. Phys. (N.Y.) **7**, 404 (1959): $F_{\{\lambda\}}(\theta)=(1/p)\sum_J(J+\frac{1}{2})\alpha_{\{\lambda\}}{}^J d_{\lambda\mu}{}^J(\theta)$. Using $-t'=4pp'\sin^2(\frac{1}{2}\theta)$ and the high-J and small-angle limit of $d_{\lambda\mu}{}^J$, namely, $d_{\lambda\mu}{}^J(\theta)\simeq J_{\mu-\lambda}[(J+\frac{1}{2})2\sin\frac{1}{2}\theta]$, we find (4) with b as given.

lengths of the interacting particles are small compared to the interaction volume. Under these conditions the low partial waves are most strongly affected by short-range interactions, and use of simple pion exchange for the low partial waves is unreasonable. Our model, then, applies for laboratory momenta higher than a few GeV/c.

Briefly our assumptions are:

(a) High partial waves, $b \gg a$, are given by the Born approximation for pion exchange; we call these partial waves long-range pion exchange.

(b) Low partial waves, $b \lesssim a$, are of the coherent-droplet-model form.

(c) The transition between these two forms is smooth.

IV. LONG-RANGE PION EXCHANGE

In this section we calculate the high-partial-wave amplitudes for pion exchange in the Born approximation. We take the Born approximation to be the Feynman amplitude for Fig. 1(a). For the reactions we consider, there is only one independent coupling mode for each vertex that satisfies Lorentz invariance and parity conservation. We choose the coupling modes given in Table I. There is only one coupling constant at each vertex. For unstable particles, we evaluate the coupling constants using the relations between the coupling constants and the decay widths given by the Feynman diagram in Fig. 1(b).

The helicity amplitudes for one-pion exchange (OPE) have the form

$$F_{\{\lambda\}}{}^{\mathrm{OPE}}(s,t) = N V_{\lambda_c\lambda_a}(s,t)\, V_{\lambda_d\lambda_b}(s,t)/(t-\mu^2), \quad (5)$$

where N is a kinematic factor,[15] μ is the pion mass, and the $V_{\lambda\mu}$ are vertex functions given in Table I. The technique for performing the partial-wave decomposition of (5) is well known.[16] With $b=(J+\frac{1}{2})/(pp')^{1/2}$ we find that, for $J \gg 1$ and $pp' \gg (\mu^2 - t_{\min})$, the partial-wave

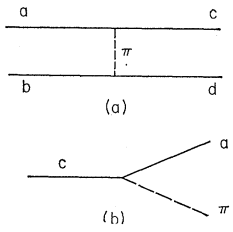

FIG. 1. Feynman diagrams: (a) for pion exchange in the process $a+b \to c+d$ and (b) for the decay $c \to a+\pi$.

[15] $F_{\{\lambda\}}$ are normalized so that

$$d\sigma/d\Omega = [1/(2S_a+1)(2S_b+1)] \sum_{\{\lambda\}} |F_{\{\lambda\}}|^2.$$

The kinematic factors are given by

$$N = (1/8\pi\sqrt{s})(p'/p)^{1/2} \quad \text{(boson-boson)},$$
$$= (1/4\pi\sqrt{s})(p'/p)^{1/2}(mm')^{1/2} \quad \text{(boson-fermion)},$$
$$= (1/2\pi\sqrt{s})(p'/p)^{1/2}(m_a m_b m_c m_d)^{1/2} \quad \text{(fermion-fermion)},$$

where m and m' are fermion masses.

[16] See, e.g., L. Durand, III, and Y. T. Chiu, Phys. Rev. **139**, B646 (1965).

TABLE I. Definitions of coupling constants and values obtained from partial widths. e_μ is a spin-1 polarization vector, $e_{\mu\nu}$ is a spin-2 polarization tensor, u and u_μ are spinors for the spin-$\frac{1}{2}$ and spin-$\frac{3}{2}$ particles, respectively. The $V_{\lambda_c\lambda_a}$ are evaluated explicitly in Appendix B.

Vertex	$V_{\lambda_c\lambda_a}$	Strength $g^2/4\pi$	Partial width[a] (MeV)
$pp\pi$	$g_{pp\pi}\bar{u}(p',\lambda')\gamma_5 u(p,\lambda)$	14.4	...
$\rho\pi\pi$	$2g_{\rho\pi\pi}e_\mu(p',\lambda')p^\mu$	2.4	125
$f^0\pi^+\pi^-$	$(4g_{f^0\pi^+\pi^-}/m_{f^0})e_{\mu\nu}(p',\lambda')p^\mu p^\nu$	2.5	94
$K^{*-}K^-\pi^0$	$2g_{K^{*-}K^-\pi^0}e_\mu(p',\lambda')p^\mu$	0.75	15
$K^{*0}K^-\pi^+$	$2g_{K^{*0}K^-\pi^+}e_\mu(p',\lambda')p^\mu$	1.50	30
$\Delta^{++}p\pi^+$	$(g_{\Delta^{++}p\pi^+}/m_\Delta)\bar{u}_\mu(p',\lambda')p^\mu u(p,\lambda)$	29.0	120

[a] Particle Data Group, Rev. Mod. Phys. **40**, 77 (1968).

amplitudes are

$$\alpha_{\{\lambda\}}{}^{\mathrm{OPE}}(b,s) = -[(-1)^{-\Delta\lambda/2}/p'] N V_{\lambda_c\lambda_a}(s,\mu^2) \times V_{\lambda_d\lambda_b}(s,\mu^2) K_{\Delta\lambda}(\mu' b), \quad (6)$$

where

$$\mu' = (\mu^2 - t_{\min})^{1/2} \quad (7)$$

and $K_n(x)$ is the modified Bessel function.[17] The quantity μ'^2 is the distance from the physical region to the pion pole. The $V_{\lambda\mu}$ are evaluated in the c.m. frame with s fixed and t continued to the unphysical point $t=\mu^2$. In our analysis, we use the central values of the resonance masses.

For $\mu' b > |\Delta\lambda|$, $\alpha_{\{\lambda\}}{}^{\mathrm{OPE}}$ has the form

$$\alpha_{\{\lambda\}}{}^{\mathrm{OPE}}(b,s) \cong R_{\{\lambda\}}{}^{\pi}(\tfrac{1}{2}\pi)^{1/2}[e^{-\mu' b}/(\mu' b)^{1/2}], \quad (8)$$

where

$$R_{\{\lambda\}}{}^{\pi} \equiv -[(-1)^{-\Delta\lambda/2}/p'] N V_{\lambda_c\lambda_a}(s,\mu^2) V_{\lambda_d\lambda_b}(s,\mu^2). \quad (9)$$

$R_{\{\lambda\}}{}^{\pi}$ is just the pion-pole residue, aside from a multiplicative factor.

In our model, the partial-wave amplitudes have the form (8) for $b > a$. We refer to these high partial waves as long-range pion exchange (LRPE). If $|\Delta\lambda| > \mu' b$, the partial waves of the Born approximation for $b \simeq a$ are larger than (8). However, we always use (8) to estimate LRPE because we believe the large values of $K_{\Delta\lambda}$ in this range of b are a consequence of unphysical singularities in Born partial-wave amplitudes at $b=0$.

The scattering amplitudes in our model have a pole at $t=\mu^2$. For elastic scattering it has been proved that if partial-wave amplitudes have the asymptotic behavior $e^{-\mu b}/(\mu b)^{1/2}$, then the scattering amplitude has a pole at $t=\mu^2$.[7] That proof can be extended to inelastic scattering. This is done simply by replacing t by t' and μ by μ'. In this way one can prove that if the partial-wave amplitudes have the asymptotic behavior

[17] *Handbook of Mathematical Functions*, edited by M. Abramowitz and I. Stegun (Dover, New York, 1965).

TABLE II. Pion helicity vertex functions in the limit $p_c \simeq p_a \simeq \infty$ with t finite.

Vertex			λ_c	λ_a	$V_{\lambda_c\lambda_a}$
1^-	0^-	0^-	1	0	$-g_{ca\pi}2\sqrt{(-\frac{1}{2}t)}$
			0	0	$g_{ca\pi}(m_a^2-m_c^2-t)/m_c$
2^+	0^-	0^-	2	0	$-(g_{ca\pi}/m_c)2t$
			1	0	$-(g_{ca\pi}/m_c)[(m_a^2-m_c^2-t)/m_c]2\sqrt{(-t)}$
			0	0	$(4g_{ca\pi}/m_c)\{(\sqrt{2}/\sqrt{3})[(m_a^2-m_c^2-t)/2m_c]^2+(t/\sqrt{6})\}$
$\frac{1}{2}^+$	$\frac{1}{2}^+$	0^-	$\frac{1}{2}$	$\frac{1}{2}$	$g_{ca\pi}(m_c-m_a)/2\sqrt{(m_cm_a)}$
			$\frac{1}{2}$	$-\frac{1}{2}$	$-g_{ca\pi}\sqrt{(-t)}/2\sqrt{(m_cm_a)}$
$\frac{3}{2}^+$	$\frac{1}{2}^+$	0^-	$\frac{3}{2}$	$-\frac{1}{2}$	$(g_{ca\pi}/m_c)[t/2\sqrt{(2m_cm_a)}]$
			$\frac{3}{2}$	$\frac{1}{2}$	$-(g_{ca\pi}/m_c)[m_c+m_a)\sqrt{(-t)}/2\sqrt{(2m_cm_a)}]$
			$\frac{1}{2}$	$-\frac{1}{2}$	$(g_{ca\pi}/m_c)\{[(m_a^2-m_c^2-t)/2m_c]-\frac{1}{2}(m_c+m_a)\}\sqrt{(-t)}/\sqrt{(6m_am_c)}$
			$\frac{1}{2}$	$\frac{1}{2}$	$[g_{ca\pi}/m_c\sqrt{(6m_cm_a)}][(m_c+m_a)[(m_a^2-m_c^2-t)/2m_c]-\frac{1}{2}t]$

$e^{-\mu' b}/(\mu' b)^{1/2}$, then the scattering amplitude has a pole at $t'=\mu'^2$. By Eqs. (2) and (7), $t'=\mu'^2$ is equivalent to $t=\mu^2$.

The LRPE contribution to the differential cross section can peak or dip at $t'=0$ depending on the relative magnitudes of the pion-pole residues in amplitudes with $\Delta\lambda=0$ compared to the residues in amplitudes with $|\Delta\lambda|\neq 0$. From (9) we see that the helicity dependence of the $R_{\{\lambda\}}{}^{\pi}$ is determined by $V_{\lambda_c\lambda_a}(s,\mu^2)$ and $V_{\lambda_d\lambda_b}(s,\mu^2)$.

In Appendix A we give the general helicity dependence of $V_{\lambda_c\lambda_a}(s,t)$ for particles of arbitrary mass, spin, and parity. We show that near $t=0$, the helicity dependence of $V_{\lambda_c\lambda_a}(s,t)$ is sensitive to m_a-m_c. For $m_a\neq m_c$ and the spins and parities of c and a arbitrary, we show that for t sufficiently small,

$$|V_{\lambda_c\lambda_a}(s,t)|_{|\lambda_c-\lambda_a|=n} > |V_{\lambda_c'\lambda_a'}(s,t)|_{|\lambda_c'-\lambda_a'|=n+1}. \quad (10)$$

For $m_a=m_c$, s_c arbitrary, and $s=0$ or $\frac{1}{2}$, we show, for t sufficiently small and the parities the same, that

$$V_{\lambda_c\lambda_a}(s,t)|_{|\lambda_c-\lambda_a|=(\text{odd})} > |V_{\lambda_c'\lambda_a'}(s,t)|_{|\lambda_c'-\lambda_a'|=(\text{even})}. \quad (11)$$

For the same conditions on the masses, spins, and t, but with the parities opposite, we show that

$$|V_{\lambda_c\lambda_a}(s,t)|_{|\lambda_c-\lambda_a|=(\text{even})} > |V_{\lambda_c'\lambda_a'}(s,t)|_{|\lambda_c'-\lambda_a'|=(\text{odd})}. \quad (12)$$

In Appendix B we give detailed expressions for the particular vertex functions that we use. Since the general expressions are complicated, we give in Table II expressions for these vertex functions in the limit $|\mathbf{p}_a|=|\mathbf{p}_c|=\infty$ with t finite.

For the unequal-mass vertices we consider, the mass difference is large compared to the pion mass. From Table II we see that for these vertices the inequality (10) is satisfied at $t=\mu^2$. The only equal-mass vertex we consider is the nucleon-nucleon vertex. For this case, when $\lambda_c=\lambda_a$, $V_{\lambda_c\lambda_a}$ is zero for all t if $|\mathbf{p}_c|=|\mathbf{p}_a|$, and is finite but very small if $|\mathbf{p}_c|\cong|\mathbf{p}_a|$. $V_{\lambda_c\lambda_a}$ is proportional to $\sqrt{(-t')}$ when $|\lambda_c-\lambda_a|=1$. At high energies in the c.m. frame for the scattering process $a+b\to c+d$, $|\mathbf{p}_c|\cong|\mathbf{p}_a|$, so that the nucleon-nucleon vertex function with $|\lambda_c-\lambda_a|=1$ dominates the vertex function with $\lambda_c=\lambda_a$.

Using (10) and the special properties of the nucleon-nucleon vertex functions, we place quasi-two-body reactions into two classes. Class I consists of reactions in which $|m_a-m_c|\gg\mu$ and $|m_b-m_d|\gg\mu$. From (10), we find that the largest $R_{\{\lambda\}}{}^{\pi}$ has $\Delta\lambda=0$ and $\lambda_a=\lambda_c$ and $\lambda_b=\lambda_d$. Class II consists of reactions with a large mass change at one vertex while the nucleon passes straight through at the other vertex. Equation (10), together with the special properties of the nucleon-nucleon vertex, leads to the result that the largest $R_{\{\lambda\}}{}^{\pi}$ has $\lambda_a=\lambda_c$ at the vertex for which $|m_a-m_c|\gg\mu$, and $|\lambda_b-\lambda_d|=1$ at the nucleon-nucleon vertex. Thus in Class-II reactions the largest $R_{\{\lambda\}}{}^{\pi}$ has $|\Delta\lambda|=1$. As we shall show, the different helicity dependence of the pion-pole residue in Class-I and Class-II reactions leads to a forward peak in the LRPE contribution in Class-I reactions and to a forward dip in Class-II reactions.

In order to calculate the effects of LRPE on differential cross sections, we must consider the low partial waves. We do this in Sec. V.

V. LOW PARTIAL WAVES

An extension of the coherent-droplet (CD) model to inelastic scattering is[18]

$$\alpha_{\{\lambda\}}{}^{\text{CD}}(b,s)=K_{\{\lambda\}}b^{|\Delta\lambda|}\int_{-\infty}^{\infty}dz\,\exp[2i\delta_i(-\infty\to z)]\times P(\mathbf{b},z)\,\exp[2i\delta_f(z\to\infty)], \quad (13)$$

where $K_{\{\lambda\}}$ is an energy-dependent constant. The factor $b^{|\Delta\lambda|}$ represents the assumption that glancing collisions

[18] This model is an extension to quasi-two-body reactions of the coherent-droplet model introduced for charge exchange by Byers and Yang (Ref. 10). We use the notation of Chou (Ref. 9). See also extensions of the droplet model to elastic scattering: T. T. Chou and C. N. Yang, Phys. Rev. **170**, 1591 (1968); and in *High Energy Physics and Nuclear Structure*, edited by G. Alexander (North-Holland, Amsterdam, 1967), pp. 348–359.

are more effective in producing helicity flips.[7] The beam direction is along the z axis. $P(\mathbf{b}, z)$ is the probability that the scattering occurs at position z and impact parameter $\mathbf{b}$. The factor $\exp[2i\delta_i(-\infty\to z)]$ gives the absorption of the beam before scattering and $\exp[2i\delta_f(z\to\infty)]$ gives the absorption after scattering. Following Chou,[9] we assume

$$P(\mathbf{b}, z)=[\rho_i(\mathbf{b}, z)\rho_f(\mathbf{b}, z)]^{1/2}, \tag{14}$$

where the $\rho(\mathbf{b}, z)$ are taken to be the hadronic matter density functions of the initial and final states. The absorption factors are given by

$$2i\delta_i(-\infty\to z)=(\text{const})\int_{-\infty}^{z} dz_1\,\rho_i(\mathbf{b}, z_1), \tag{15}$$

with an analogous expression for δ_f. The δ are normalized such that $\delta(-\infty\to\infty)$ is the elastic phase shift.

Elastic scattering information is available for Kp, πp, and pp so that the $\int_{-\infty}^{\infty}\rho_i(\mathbf{b}, z)\,dz$ are approximately known. However, there are no elastic scattering data for the final states ρp, $K^*(890)p$, $\rho\Delta$, $f^0\Delta^{++}$, and $p\Delta$. In the absence of this information we take

$$\rho_{\pi p}=\rho_{MB} \quad\text{and}\quad \rho_{pp}=\rho_{BB}. \tag{16}$$

The elastic scattering data that are available indicate that Eq. (16) is approximately true for the Kp and πp systems. Equation (16) is sufficient for our analysis because our amplitudes in the small t' region are not sensitive to detailed features of the density functions.

With these approximations (13) reduces to the original form of the coherent-droplet model introduced for charge exchange:

$$\alpha_{\{\lambda\}}{}^{\mathrm{CD}}(b, s)=K_{\{\lambda\}}{}^{\mathrm{CD}}(b/a)^{|\Delta\lambda|}\exp(2i\delta_{\mathrm{el}})\,2i\delta_{\mathrm{el}}, \tag{17}$$

where $K_{\{\lambda\}}{}^{\mathrm{CD}}$ is a dimensionless constant which can depend on energy. The elastic phase shifts are conveniently parametrized by

$$\exp(2i\delta_{\mathrm{el}})=[1-c\exp(-b^2/a^2)]. \tag{18}$$

From the elastic scattering data,[19] the meson-baryon elastic parameters are determined to be approximately

$$a=4.5\ (\mathrm{GeV}/c)^{-1}, \qquad c=0.58, \tag{19}$$

while the baryon-baryon parameters are approximately

$$a=4.5\ (\mathrm{GeV}/c)^{-1}, \qquad c=0.91. \tag{20}$$

For the droplet model to be applicable it is necessary that there be coherence of phase over the interaction volume.[10] That is, the phase shift of the initial-state particles in passing through the interaction volume and the phase shift of the final-state particles should differ by less than π. The condition which ensures coherence of phase is

$$|\,m_a{}^2+m_b{}^2-m_c{}^2-m_d{}^2\,|\,a(p_{1\mathrm{ab}})^{-1}\ll\pi. \tag{21}$$

For the most inelastic reaction that we consider, namely, $\pi^+p\to f^0\Delta^{++}$, this requires $p_{1\mathrm{ab}}$ to be 8 GeV/c or greater.

To join the exponential tail of LRPE (8) smoothly to the droplet amplitudes, we use an interpolation similar to that introduced by Byers[7]:

$$\alpha_{\{\lambda\}}{}^{\pi}(b, s)=R_{\{\lambda\}}{}^{\pi}(1-\alpha_{\mathrm{el}})(\tfrac{1}{2}\pi)^{1/2}\times\left(\frac{b^2}{b^2+a^2}\right)^{|\Delta\lambda|/2}\frac{\exp[-\mu'(b^2+a^2)^{1/2}]}{[\mu'(b^2+a^2)^{1/2}]^{1/2}}, \tag{22}$$

where [see Eq. (18)]

$$\alpha_{\mathrm{el}}=c\exp(-b^2/a^2). \tag{23}$$

For $b\gg a$ these amplitudes have the required asymptotic behavior (8), while for $b<a$ they are smooth functions of b similar in shape to the droplet amplitudes. The absorption factor $(1-\alpha_{\mathrm{el}})$ and the factor

$$[b^2/(b^2+a^2)]^{|\Delta\lambda|/2}$$

are included to make these amplitudes similar in shape to the droplet amplitudes at small b.

Since the droplet parameters $K_{\{\lambda\}}{}^{\mathrm{CD}}$ are unknown and must be determined from experiment, we must check in each reaction that the interpolation (22) does in fact lead to a smooth joining of droplet and pion amplitudes. For all the reactions we consider, (22) does lead to a smooth joining.

VI. MODEL AMPLITUDES

Adding (22) and (17), we get the partial-wave amplitudes of the droplet model with LRPE, namely,

$$\alpha_{\{\lambda\}}(b, s)=\alpha_{\{\lambda\}}{}^{\mathrm{CD}}(b, s)+\alpha_{\{\lambda\}}{}^{\pi}(b, s). \tag{24}$$

We emphasize that only the second term contains LRPE. At large b, this term is uniquely determined by the pion-pole residue. This term is real for all b. At small b, $\alpha_{\{\lambda\}}$ has the coherent-droplet-model form. Different interpolations of the long-range-pion effect into the small-b region affect the behavior of $\alpha_{\{\lambda\}}$ between $b\lesssim a$ and $b\gg a$. The main effect of different choices of interpolation is that the real part of $\alpha_{\{\lambda\}}$ is distributed differently between $\mathrm{Re}\alpha_{\{\lambda\}}{}^{\mathrm{CD}}$ and $\alpha_{\{\lambda\}}{}^{\pi}$. A particular choice of interpolation serves to define $\mathrm{Re}K_{\{\lambda\}}{}^{\mathrm{CD}}$. We found that different smooth interpolations do not produce significant changes in the behaviors of our amplitudes at small $-t'$. Therefore, our assumption that the large-impact-parameter collisions are dominated by pion exchange has consequences that are insensitive to the detailed features of our model.

The scattering amplitudes of our model, at high energy and small t', are given by[20]

$$F_{\{\lambda\}}(s, t')=p'K_{\{\lambda\}}{}^{\mathrm{CD}}f_{\Delta\lambda}{}^{\mathrm{CD}}(t')+p'R_{\{\lambda\}}{}^{\pi}f_{\Delta\lambda}{}^{\pi}(s, t'), \tag{25}$$

[19] K. J. Foley, S. J. Lindenbaum, W. A. Love, S. Ozaki, J. J. Russell, and L. C. L. Yuan, Phys. Rev. Letters **10**, 376 (1963); **11**, 503 (1963).

[20] For our numerical calculations for each helicity flip $\Delta\lambda$, we found the amplitude which has the largest pion-pole residue. We used the exact partial-wave sum to calculate this amplitude. We used this amplitude and Eq. (25) to define $f_{\Delta\lambda}{}^{\mathrm{CD}}$ and $f_{\Delta\lambda}{}^{\pi}$.

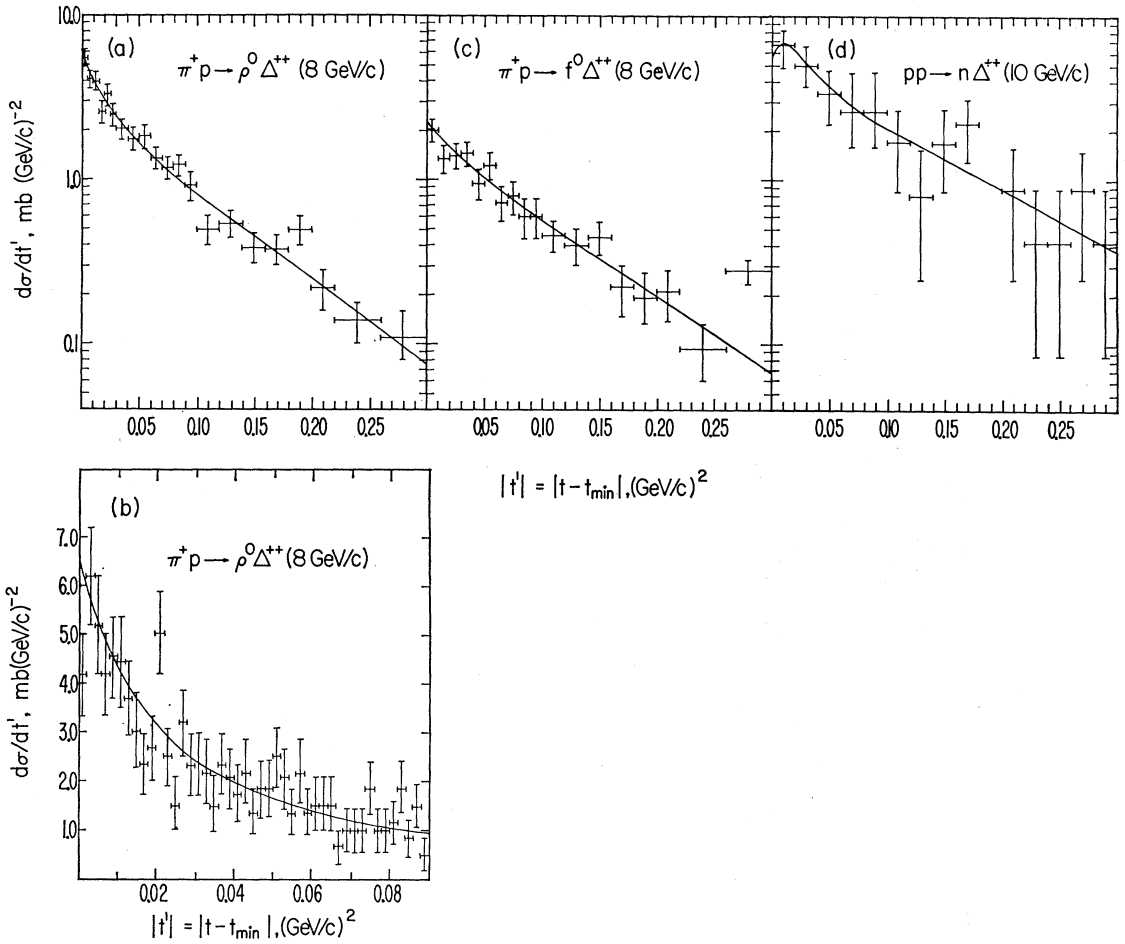

FIG. 2. Fits to the data: (a) and (b) for $\pi^+p \to \rho^0\Delta^{++}$ at 8 GeV/c; (c) for $\pi^+p \to f^0\Delta^{++}$ at 8 GeV/c; (d) for $pp \to n\Delta^{++}$ at 10 GeV/c. The parameters for these fits are given in Table III. The data in (a), (b), and (c) are from Refs. 1 and 2; the data in (d) are from Ref. 12.

where

$$f_{\Delta\lambda}{}^{\mathrm{CD}}(t') = \int b\, db\, J_{\Delta\lambda}(b\sqrt{-t'})\,(b/a)^{|\Delta\lambda|}\exp(2i\delta_{\mathrm{el}})\,2i\delta_{\mathrm{el}} \tag{26}$$

and

$$f_{\Delta\lambda}{}^{\pi}(s,t') = \int b\, db\, J_{\Delta\lambda}(b\sqrt{-t'})\,(1-\alpha_{\mathrm{el}})\,(\tfrac{1}{2}\pi)^{1/2} \times\left(\frac{b^2}{b^2+a^2}\right)^{|\Delta\lambda|/2}\frac{\exp[-\mu'(b^2+a^2)^{1/2}]}{[\mu'(b^2+a^2)^{1/2}]^{1/2}}. \tag{27}$$

The $f_{\Delta\lambda}{}^{\mathrm{CD}}$ and $f_{\Delta\lambda}{}^{\pi}$ are real functions. The $f_{\Delta\lambda}{}^{\mathrm{CD}}$ functions depend only on t'. The presence of μ' in (27) yields some energy dependence for the $f_{\Delta\lambda}{}^{\pi}$ functions; the $f_{\Delta\lambda}{}^{\pi}$ functions increase with decreasing μ', and the peaking near $t'=0$ gets sharper. As $s\to\infty$, μ' decreases to μ.

In Appendix C we give another interpolation of LRPE to small b which allows the integral in (27) to be evaluated analytically. This form is particularly convenient for numerical estimates of the shapes and magnitudes of the $f_{\Delta\lambda}{}^{\pi}$ for small t'. The expressions in Appendix C are also convenient for considering the energy dependence of $f_{\Delta\lambda}{}^{\pi}(s,t')$.

Since the $f_{\Delta\lambda}{}^{\mathrm{CD}}$ and $f_{\Delta\lambda}{}^{\pi}$ depend on helicities only through $\Delta\lambda$, the differential cross section in our model has the simple form

$$\frac{d\sigma}{dt'} = \sum_{n=0}^{n_{\max}} |\, \mathfrak{R}_n{}^{\pi} f_n{}^{\pi}(s,t') + C_n \exp(i\phi_n) f_n{}^{\mathrm{CD}}(t')\,|^2, \tag{28}$$

where $n = |\,\Delta\lambda\,|$ and $n_{\max}=1$ for $0\tfrac{1}{2}\to 0\tfrac{1}{2}$, $n_{\max}=2$ for $0\tfrac{1}{2}\to 1\tfrac{1}{2}$, etc. The $\mathfrak{R}_n{}^{\pi}$ are given by the residues $R_{\{\lambda\}}{}^{\pi}$ as follows:

$$\mathfrak{R}_n{}^{\pi} = \{(p'/p)[\pi/(2s_a+1)\,(2s_b+1)] \times \sum_{\lambda_a,\lambda_b,\lambda_c,\lambda_d} |\, R_{\{\lambda\}}{}^{\pi}\,|^2 \delta_{n,|\Delta\lambda|}\}^{1/2}, \tag{29}$$

TABLE III. Residues and parameters used to calculate the theoretical curves. They are dimensionless (see text). The $\mathcal{R}_n^{\pi}$ are determined from known decay widths. The C_n and $\cos\phi_n$ are droplet-model parameters chosen to fit the data. (···) indicates the parameter was not used.

Reaction (momentum)	$\mathcal{R}_0^{\pi}$	C_0	$\cos\phi_0$	$\mathcal{R}_1^{\pi}$	C_1	$\cos\phi_1$	$\mathcal{R}_2^{\pi}$	C_2	$\cos\phi_2$	$\mathcal{R}_3^{\pi}$	$\mathcal{R}_4^{\pi}$
$\pi^+p\to\rho^0\Delta^{++}$(8 GeV/$c$)	0.412	0.51	−0.55	0.363	0.16	···	0.115	0.072	···	0.075	···
$\pi^+p\to f^0\Delta^{++}$(8 GeV/c)	1.18	0.34	−0.87	1.24	0.13	···	0.556	···	···	0.031	0.019
$\pi^-p\to\rho^0n$ (11.2 GeV/c)	0.0250	0.28	0.0	0.0768	0.16	0.75	0.0203	0.095	···	···	···
$\pi^+p\to\rho^+p$ (8.0 GeV/c)	0.0283	0.27	−0.725	0.0771	0.30	···	0.0207	0.088	···	···	···
$K^-p\to K^{*0}(890)n$ (10.0 GeV/c)	0.0206	0.088	−0.5	0.0563	0.088	···	0.0179	0.019	···	···	···
$K^-p\to K^{*-}(890)p$ (10.0 GeV/c)	0.0103	0.095	−0.75	0.0282	0.34	···	0.00895	0.20	···	···	···
$pp\to\Delta^{++}n$ (10 GeV/c)	0.0815	0.44	···	0.220	0.47	···	0.0792	0.25	···	0.005	···

and the C_n are related to the $K_{\{\lambda\}}^{\mathrm{CD}}$ by

$$C_n=\{(p'/p)[\pi/(2s_a+1)(2s_b+1)]\times\sum_{\lambda_a,\lambda_b,\lambda_c,\lambda_d}|K_{\{\lambda\}}^{\mathrm{CD}}|^2\delta_{n,|\Delta\lambda|}\}^{1/2}. \quad (30)$$

To get information on the individual droplet parameters $K_{\{\lambda\}}^{\mathrm{CD}}$, one must study density-matrix elements. The differential cross section depends only on the cosine of the phases ϕ_n; the $\cos\phi_n$ are given by

$$\cos\phi_n=(p'/p)[\pi/(2s_a+1)(2s_b+1)](\mathcal{R}_n^{\pi}C_n)^{-1}\times\sum_{\lambda_a,\lambda_b,\lambda_c,\lambda_d}R_{\{\lambda\}}^{\pi}\,\mathrm{Re}(K_{\{\lambda\}}^{\mathrm{CD}})\delta_{n,|\Delta\lambda|}. \quad (31)$$

Although, from their definition, the $\cos\phi_n$ can vary from -1 to $+1$, our requirement that the transition between LRPE and the coherent-droplet form be smooth in certain cases restricts the variation to a smaller range.

Equation (28) is a simple and physical parametrization of the differential cross section which we use to analyze the data on quasi-two-body reactions with pion exchange. The pion amplitudes $\mathcal{R}_n^{\pi}f_n^{\pi}(s,t')$ are sharply peaked at small t' and are responsible for any structure in the differential cross section for $-t'\lesssim\mu'^2$. The droplet amplitudes $C_n\exp[i\phi_n]f_n^{\mathrm{CD}}(t')$ describe the effects of the low partial waves. They give relatively slowly varying contributions to the differential cross section. These contributions dominate for $-t'\gg\mu'^2$.

The rapid variation of the differential cross section for $-t'<\mu'^2$ is model independent. The behavior of the differential cross section in this region follows from our assumptions that pion exchange dominates large-impact-parameter collisions and that the partial-wave amplitudes are smooth and slowly varying functions of b. Near $t'=0$, one can regard the coherent-droplet model as just a convenient parametrization of the large-$(-t')$ data which gives an estimate of the low-partial-wave contributions near $t'=0$.

Our calculated amplitudes for $-t'\gg\mu'^2$ can be used to test the coherent-droplet model. In this region LRPE contributions are small. The larger the value of $-t'$ the more sensitive the amplitudes are to the detailed features of the low partial waves.

VII. RESULTS

Here we present our fits to the data and our analysis of the seven reactions (A)–(G). We consider first the two Class-I reactions (A)–(B). In Sec. IV we showed that for Class-I reactions the pion-pole residue is largest in the helicity amplitude with $\Delta\lambda=0$ and $\lambda_a=\lambda_c$ and $\lambda_b=\lambda_d$. The LRPE contribution to this amplitude peaks sharply at $t'=0$.

A. $\pi^+p\to\rho^0\Delta^{++}$ at 8 GeV/c

The Aachen-Berlin-CERN data[4] displayed in Figs. 2(a) and 2(b) clearly show a sharp rise for $-t'<0.03$ (GeV/c)^2. In Figs. 2(a) and 2(b), we show a fit to the data using our model. The fit shown is a visual fit to the data with the parameters C_0, C_1, and C_2 chosen to fit the $0.3\geq-t'\gtrsim0.07$ (GeV/c)^2 data and $\cos\phi_0$ chosen to fit the shape and magnitude of the forward spike. In our analysis we found C_3 to be small. Also, we found the effect of interference between LRPE and the droplet amplitudes for $|\Delta\lambda|=1$ and $|\Delta\lambda|=2$ to be small compared to the contributions of $\Delta\lambda=0$ amplitudes. For simplicity, we chose C_3, $\cos\phi_1$, $\cos\phi_2$, and $\cos\phi_3$ to be zero. The residues and parameter values for our fit are given in Table III. For $-t'>0.3$ (GeV/c)^2, the coherent-droplet model fails to account for the data (see Fig. 5). We expect the coherent-droplet model to work over a larger region of t' at higher energies, when the condition for phase coherence (21) is better satisfied.

In this reaction, there are high-statistics data for $-t'<0.03$ (GeV/c)^2 [see Fig. 2(b)]. The shape and magnitude of the differential cross section in this region depend sensitively on the interference parameter $\cos\phi_0$. This parameter gives information about the phases of the small-b partial waves. Our fit shows that, roughly speaking, there is no interference between LRPE and the small-b partial waves. Three different helicity amplitudes contribute to $\mathcal{R}_0^{\pi}$, C_0, and $\cos\phi_0$. LRPE contributes mainly to the amplitude with $\{\lambda\}=(0,\frac{1}{2};0,\frac{1}{2})$. If we assume that this amplitude dominates the $\Delta\lambda=0$ contribution to the differential cross section, our fit implies that the small-b partial waves are mainly imaginary. Since the high partial waves are real, the

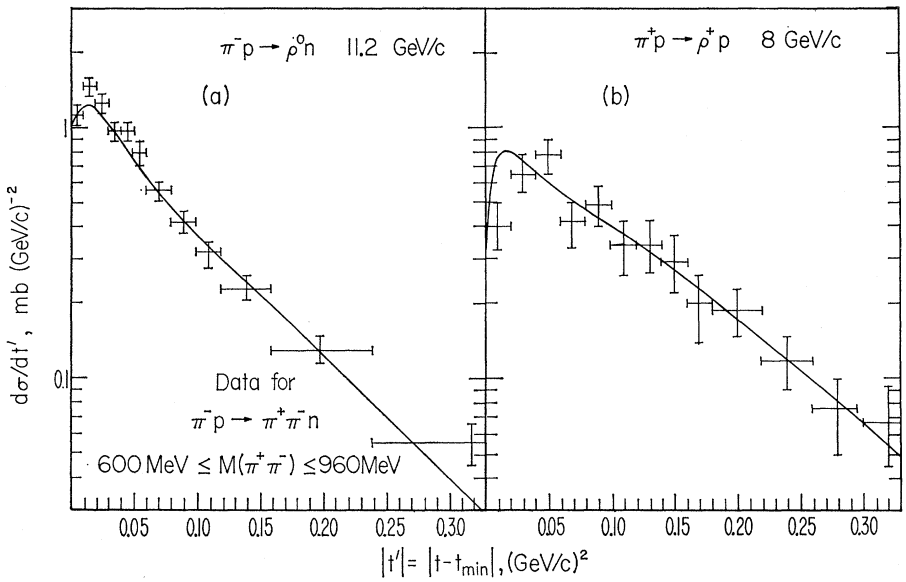

FIG. 3. (a) A fit to the data for $\pi^- p \to \pi^+ \pi^- n$ at 11.2 GeV/c. The theoretical curve includes only P-wave $\pi^+\pi^-$ production. The experimental data may include some S-wave production (see text). The data are from Ref. 3. (b) A fit to the data for $\pi^+ p \to \rho^+ p$ at 8 GeV/c. The data are from Ref. 1. The parameters for these fits are given in Table III.

phases of the partial-wave amplitudes must vary rapidly near the surface of the interaction volume. If the droplet contributions to other $\Delta\lambda = 0$ amplitudes are large, we can make no conclusions about the phase variation.

Another way to see that the data correspond to little interference between LRPE and the small-b partial waves is to note the following: The partial-wave amplitudes of pion exchange (6) for $b \geq 7$ (GeV/c)$^{-1}$ contribute 5.3 mb (GeV/c)$^{-2}$ to the differential cross section at $t' = 0$. LRPE, defined to be these partial waves, therefore accounts for the magnitude of the spike. LRPE also accounts for its slope near $t' = 0$.

Our analysis shows that any simply modified OPE model in which the low partial waves differ from OPE in magnitude but are mainly real cannot account for these data.[21]

B. $\pi^+ p \to f^0 \Delta^{++}$ at 8 GeV/c

The 8-GeV/c data, shown in Fig. 2(c), show no structure for $-t' < 0.1$ (GeV/c)^2. In particular, they give no evidence for a spike as seen in $\pi^+ p \to \rho^0 \Delta^{++}$.

In this reaction, at 8 GeV/c the distance from the physical region to the pion pole is large compared to the pion mass squared; that is, $\mu'^2 \simeq 6\mu^2$. One might thus expect the pion effect to be small. The differential cross section in the simple Born approximation, however, is five times larger than the observed differential cross section at $t' = 0$. Furthermore, the discrepancy increases as $-t'$ increases.

LRPE, however, is consistent with the data. The partial-wave amplitudes of pion exchange (6) for $b \geq 7$ (GeV/c)$^{-1}$ contribute only 1.8 mb (GeV/c)$^{-2}$ to the differential cross section at $t' = 0$. From Eq. (8), we see that $(\mu')^{-1}$ can be regarded as the range of the pion-exchange interaction. The pion effect in $\pi^+ p \to f^0 \Delta^{++}$ at 8 GeV/c is therefore broader than in $\pi^+ p \to \rho^0 \Delta^{++}$ at the same energy. Because interference is possible between LRPE and the small-b partial waves, the pion effect in the differential cross section at $t' = 0$ can be smaller or larger than 1.8 mb (GeV/c)$^{-2}$. A rise of 1.5 mb (GeV/c)$^{-2}$ for $-t' < 0.04$ (GeV/c)^2 is certainly consistent with the data.

Our model does not provide a particularly convenient parametrization for the differential cross section in this reaction because μ' is large. LRPE contributions to scattering amplitudes are important in a region of t' characterized by μ'^2. At 8 GeV/c, μ'^2 is approximately 0.11 (GeV/c)^2. Interference effects between LRPE and the small-b partial waves at this energy can be important in the entire range $-t' < 0.3$ (GeV/c)^2. Because the final-state particle spins are large and interference effects are important over such a large range of t', $d\sigma/dt'$ in our model (28) can depend importantly on too many parameters (five droplet and five interference) to allow a meaningful detailed fit to the available data. However, for $-t' < 0.1$ (GeV/c)^2 the dominant contributions to $d\sigma/dt'$ come from $|\Delta\lambda| = 0,1$ amplitudes. Possible interference effects in $\Delta\lambda = 0$ amplitudes are much larger than those in $|\Delta\lambda| = 1$ amplitudes. In Fig. 2(c) we show a curve given by the model when only the three parameters C_0, C_1, and $\cos\phi_0$ are used. Since there are so many parameters in the coherent-droplet model for this reaction, these data do not provide a good test for the model. Our curve shows only that the coherent-droplet model with LRPE is consistent with these data. While these data are consistent with LRPE, they give no evidence for LRPE because they show no structure near $t' = 0$. (See Sec. VIII for the possible effects of LRPE in this reaction at higher energies.)

[21] See, e.g., J. D. Jackson, Rev. Mod. Phys. **37**, 484 (1965); J. D. Jackson, J. T. Donahue, K. Gottfried, R. Keyser, and B. E. Y. Svensson, Phys. Rev. **139**, B428 (1965).

For $-t'>0.3$ $(\mathrm{GeV}/c)^2$, the model cannot account for the data. For $-t'>0.3$ $(\mathrm{GeV}/c)^2$ the data show a broadening of slope which cannot be explained by the coherent-droplet model. However, we expect the coherent-droplet model to give good fits to the data over a wider region of $-t'$ at higher energies when the mass changes are smaller relative to the total energy.

Next we consider reactions in Class II, that is, reactions for which $m_a \neq m_c$ while the nucleon passes straight through at the other vertex. For these reactions, we showed in Sec. IV that the pion-pole residue is largest for those helicity amplitudes for which $\lambda_a=\lambda_c$ and $|\lambda_b-\lambda_d|=1$. As a consequence, for the reactions we consider, the LRPE contribution always dips in the forward direction. If LRPE dominates at small $-t'$, the differential cross section dips in the forward direction and peaks near $t'\simeq-\mu^2$. The details of the curvature at small $-t'$ depend on the relative phases and magnitudes of LRPE and the small-b partial waves, as is shown in the various cases we discuss. Our model cannot predict if the LRPE effect dominates at small $-t'$. However, using the large-$(-t')$ data, we can use the model to predict whether the LRPE effect dominates.

For the reactions in Class II, the change in wavelengths of the particles between initial and final states is not as great as for the reactions in Class I. It is characteristic of Class-II reactions that the coherent-droplet model fits the data over a larger range of t'.

C. $\pi^- p \to \rho^0 n$ at 11.2 GeV/c

The data shown in Fig. 3(a) indicate the LRPE effect characteristic of reactions in Class II. The data include non-ρ^0 background. Our fit to the data includes only the long-range-pion contribution to ρ^0 production. The parameter values for our curve are given in Table III. Our curve has the shape indicated by the data, but for $-t'<0.06$ $(\mathrm{GeV}/c)^2$ it tends to be low. We can account for this discrepancy by noting that LRPE can contribute to S-wave $\pi^+\pi^-$ production. We estimate this effect by calculating the LRPE contribution to the production of an S-wave $\pi^+\pi^-$ resonance near the mass of the ρ using the Feynman diagram in Fig. 1(a). There are only two independent helicity amplitudes for this reaction, $\Delta\lambda=0$ and 1. Pion exchange contributes only to the $|\Delta\lambda|=1$ amplitude. The t' dependence of the LRPE contribution to the $|\Delta\lambda|=1$ amplitude in S-wave $\pi^+\pi^-$ production is the same as the corresponding contribution to the $|\Delta\lambda|=1$ amplitude in ρ^0 production. If the LRPE effect in S-wave $\pi^+\pi^-$ production is 20% of the $|\Delta\lambda|=1$ contribution in ρ production, its inclusion improves the fit for $-t'<0.06$ $(\mathrm{GeV}/c)^2$.

D. $\pi^+ p \to \rho^+ p$ at 8 GeV/c

Owing to isospin conservation, the LRPE effect in this reaction is smaller by $\frac{1}{2}$ than it is in the $\pi^- p \to \rho^0 n$ at the same energy. However, owing to the energy dependence of the pion-exchange interaction, the LRPE effect is as strong in $\pi^+ p \to \rho^+ p$ at 8 GeV/c as it is in $\pi^- p \to \rho^0 n$ at 11 GeV/c. Since the large-$(-t')$ data are of the same order of magnitude as in $\pi^- p \to \rho^0 n$, we expect to see a LRPE effect in the data. The LRPE effect always has its maximum near $t'=-0.015$ $(\mathrm{GeV}/c)^2$ and dips in the forward direction. The data displayed in Fig. 3(b) are consistent with this behavior. The curve in Fig. 3(b) indicates the type of structure our model gives. The interference parameters $\cos\phi_0$ and $\cos\phi_1$ are not well determined by the data. Since the contributions of droplet and LRPE amplitudes are like those in $\pi^- p \to \rho^0 n$, a different choice of $\cos\phi_0$ and $\cos\phi_1$ could give similar structure to that shown in Fig. 3(a). The values of the C_n we found from the large-$(-t')$ data and the values of $\cos\phi_n$ we chose for the fit shown in Fig. 3(b) are given in Table III. We note that the data seem to indicate peaking near $t'=-0.05$ $(\mathrm{GeV}/c)^2$. Such structure could not be accounted for by our model.

E. $pp \to n\Delta^{++}$ at 10 GeV/c

The analysis of this reaction is similar to that of the preceding two. Again the pion contribution peaks near $t'=-0.015$ $(\mathrm{GeV}/c)^2$ and dips in the forward direction. In this reaction, owing to large statistical errors, the large-$(-t')$ data allow only a rough estimate of the small-b partial-wave-amplitude contributions to the differential cross section near $t'=0$ [see Fig. 2(d)]. We find that LRPE and short-range interactions give comparable contributions for $-t'<0.04$ $(\mathrm{GeV}/c)^2$. For most parameter values, we find structure like that shown by the curve in Fig. 2(d). The detailed features of the curve, such as the depth of the dip and the curvature, depend on the particular parameter values chosen. More reliable estimates of the parameters require data of higher statistical precision. The parameter values for the curve shown are given in Table III.

Note that in this reaction LRPE produces a dip in the forward direction. In np charge exchange, on the other hand, it produces a sharp peak. This different behavior follows from the different mass structure of these reactions and the kinematic properties of pion helicity vertex functions (see Sec. IV). The helicity must flip at both pion vertices in np charge exchange. LRPE contributes to $|\Delta\lambda|=0$ and 2 amplitudes. The helicity-flip-zero contribution dominates near $t'=0$ and produces the spike.

F. $K^- p \to K^{*0}(890) n$ at 10 GeV/c

Using the $-t'>0.1$ $(\mathrm{GeV}/c)^2$ data, we estimate the small-b partial-wave-amplitude contributions to the differential cross section near $t'=0$ to be 0.1 mb $(\mathrm{GeV}/c)^{-2}$. The magnitude of the long-range pion contribution at $t'=-0.015$ $(\mathrm{GeV}/c)^2$ is approximately 0.26 mb $(\mathrm{GeV}/c)^{-2}$. Thus, we find that the LRPE contribution dominates the $-t'<0.05$ $(\mathrm{GeV}/c)^2$ differential cross section. The LRPE effect is so large that

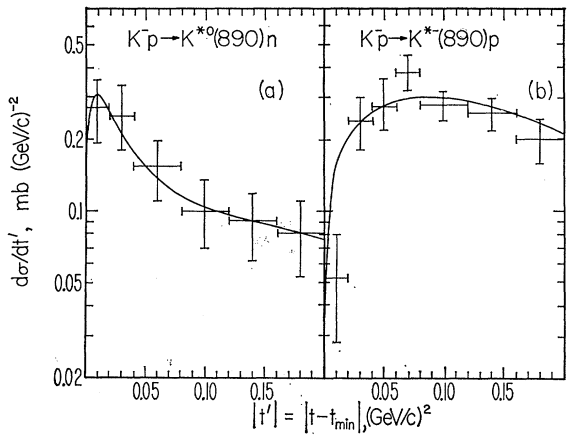

FIG. 4. Our fits to the data: (a) for $K^-p\to K^{*0}(890)n$ and (b) for $K^-p\to K^{*-}(890)p$ at 10 GeV/c in the region $0\leq -t'\leq 0.2$ (GeV/c)^2. These fits at larger $-t'$ are displayed in Fig. 5. The data are from Ref. 11. The parameters are given in Table III.

there is some LRPE effect in the whole range $-t'<4\mu^2$. LRPE produces a rise for $-t'<0.08$ (GeV/c)^2, peaking near $-t'<0.015$ (GeV/c)^2, and a dip in the forward direction. These features are illustrated in our fit shown in Fig. 4(a). The parameter values for our fit are given in Table III.

Detailed features of our fit, such as the depth of the dip, the height of the maximum, and the curvature from $0.02>-t'>0.1$ (GeV/c)^2 depend on the parameters and might change with higher statistics and a better determination of the parameters. The qualitative features of the curve, the rise for $-t'<0.1$ (GeV/c)^2, the peak near $t'=-0.015$ (GeV/c)^2, and the dip in the forward direction, follow only from the magnitude of the large-$(-t')$ data and the fact that for $-t'<0.02$ (GeV/c)^2, $d\sigma/dt'<3.5$ mb (GeV/c)$^{-2}$, as indicated by the data. The model gives no dip in the forward direction, only in the extreme case that $\cos\phi_0=+1$ and $\cos\phi_1=-1$. These conditions imply that the low partial waves with $\Delta\lambda=0$ are real and in phase with the high partial waves while the $|\Delta\lambda|=1$ low partial waves are real and 180° out of phase with the high partial waves. This extreme case occurs for $d\sigma/dt'\simeq 4$ mb (GeV/c)$^{-2}$ at $t'=0$. Thus, for $K^-p\to K^{*0}(890)n$, the model predicts a dip for $-t'<0.01$ (GeV/c)^2 on the basis only of the large-$(-t')$ data and a lower limit for $d\sigma/dt'$ at $t'=0$ given by the data. Since the entire dip is in the first bin of the data, this prediction of the model requires higher statistics for confirmation.

G. $K^-p\to K^{*-}(890)p$ at 10 GeV/c

In this reaction, by isospin conservation, the LRPE contribution is four times smaller than in $K^-p\to K^{*0}(890)n$. The $-t'>0.05$ (GeV/c)^2 data require much larger small-b partial-wave-amplitude contributions to the differential cross section in this reaction. At small $-t'$, the LRPE contributions are swamped by the small-b contributions. In Fig. 4(b) we present our fit to the data. The parameter values for the fit are given in Table III.

The depth of the dip is controlled mainly by the parameter $\cos\phi_0$. Our fit corresponds to large destructive interference between LRPE and small-b partial waves in the $\Delta\lambda=0$ partial-wave amplitudes. However, good fits to the present data are obtained for any value of $\cos\phi_0$. For $\cos\phi_0=+1$, $d\sigma/dt'$ would be approximately 0.2 mb (GeV/c)$^{-2}$ at $t'=0$. For $-t'>0.05$ (GeV/c)^2, the effects of varying $\cos\phi_0$ are negligible. In this reaction the long-range pion effect is too small to be detected with the available data. The peak in the data near $t'=-0.1$ (GeV/c)^2 and the dip in the forward direction imply large contributions to the differential cross section from $|\Delta\lambda|=1$ droplet amplitudes.

To summarize, LRPE can produce both dips and peaks characterized by a width μ'^2. In every reaction we considered, the data near $t'=0$ are consistent with the presence of LRPE. Only for $\pi^+p\to\rho^0\Delta^{++}$ at 8 GeV/c, however, is the detailed structure caused by LRPE firmly established. In the other reactions higher statistics are required.

Our good fits to the data for $0.3>-t'>0.1$ (GeV/c)^2 indicate that the coherent-droplet model describes approximately the partial-wave amplitudes for $b<a$. The coherent-droplet model is a model for scattering at infinite energies. At finite energies, the mass changes in the reactions we consider partly destroy the coherence of phase over the interaction volume. In Fig. 5 we compare the coherent-droplet model with the data over a large range of $-t'$ for the reactions $\pi^+p\to\rho^0\Delta^{++}$, $\pi^+p\to f^0\Delta^{++}$, $\pi^+p\to\rho^+p$, $K^-p\to K^{*0}(890)n$, and $K^-p\to K^{*-}(890)p$. (The data points for small $-t'$ are omitted because they are shown in previous figures.) In the first two reactions the mass changes are large. In these reactions the data deviate from the coherent-droplet form for $-t'>0.3$ (GeV/c)^2. In the remaining reactions, there is a mass change at only one vertex. In these reactions the coherent-droplet model fits the data over a larger range of $-t'$. As the energy increases, we expect the deviations of the data from the coherent-droplet form to occur at larger values of $-t'$ for all these reactions.

In Sec. VIII we discuss the energy dependence of LRPE.

VIII. ENERGY DEPENDENCE

Before we consider the energy dependence of the LRPE contribution to the differential cross section, we review briefly the well-known energy dependence of pion exchange in the simple Born approximation. For reactions with one independent coupling mode at each pion vertex, the differential cross section for pion exchange in the Born approximation has the form

$$d\sigma/dt=(G/p_{1\mathrm{ab}}^2)[1/(t-\mu^2)^2]\times[t-(m_a-m_c)^2]^{\eta_{ac}-}[t-(m_a+m_c)^2]^{\eta_{ac}+}\times[t-(m_b-m_d)^2]^{\eta_{bd}-}[t-(m_b+m_d)^2]^{\eta_{bd}+}. \quad (32)$$

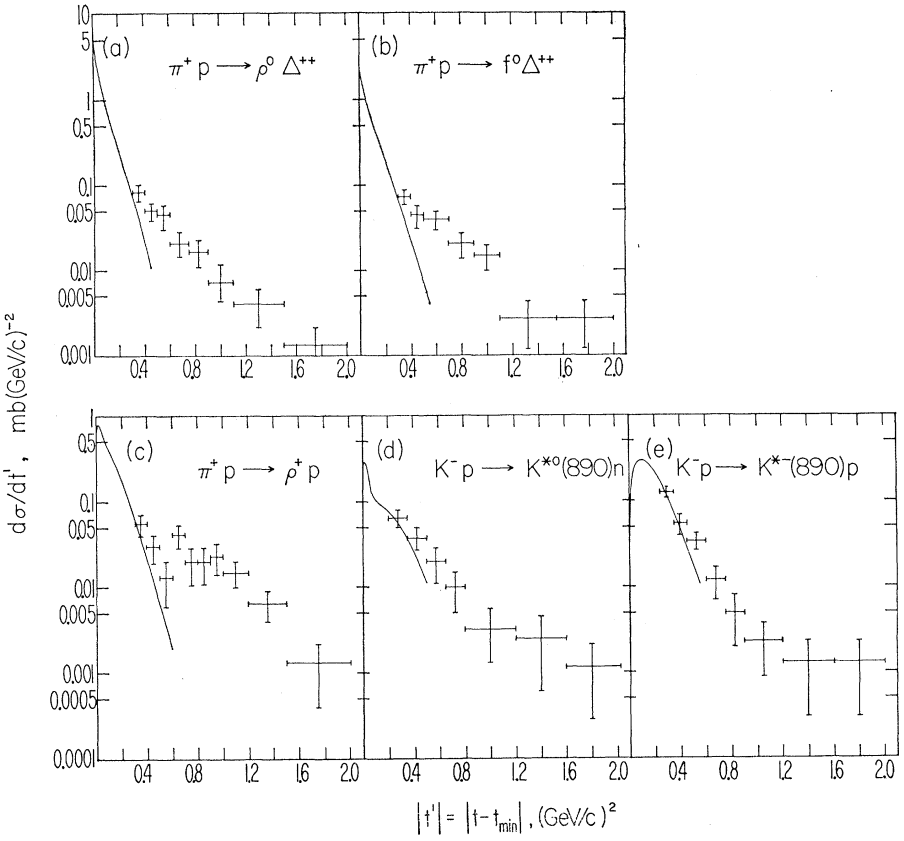

FIG. 5. Deviation of our model from the data at large $-t'$. The small-$(-t')$ data points are given in the preceding figures. All the available data for the two reactions omitted here are displayed in Figs. 2(d) and 3(a).

Here G is independent of s and t. It depends on coupling constants and the masses, spins, and parities of particles a, b, c, and d. The powers $\eta_{ac}^{\pm}$ and $\eta_{bd}^{\pm}$ are integers that depend on the spins and parities of particles ac and bd, respectively. Expressions for these factors have been given, for example, by Jackson and Hite[22] and by Frampton.[22] At fixed t, $d\sigma/dt$ in (32) decreases with increasing energy like p_{lab}^{-2}. For Class-I reactions t and t' are different at finite energies. For these reactions it is interesting to consider (32) at fixed t'. For Class-I reactions, a fixed value of t' corresponds to values of $-t$ which decrease with increasing energy. For Class-I reactions in which $(m_a-m_c)^2 \gg \mu^2$ and $(m_b-m_d)^2 \gg \mu^2$, the differential cross section peaks sharply for $-t<\mu^2$ and is concave. Thus, as the energy increases, the Born approximation at fixed t' decreases more slowly than p_{lab}^{-2} and the peaking near $t'=0$ becomes sharper.

We consider next the energy dependence of LRPE. At large b, the partial waves of pion exchange are given by Eq. (8):

$$\alpha_{\{\lambda\}}{}^{\mathrm{OPE}}(b,s) \cong R_{\{\lambda\}}{}^{\pi}(\tfrac{1}{2}\pi)^{1/2} \exp(-\mu' b)/(\mu' b)^{1/2}. \quad (8)$$

When the range of the pion-exchange interaction μ'^{-1} is energy independent, the energy dependence of LRPE is determined by the factor $R_{\{\lambda\}}{}^{\pi}$ and is the same as in the Born approximation. For Class-II reactions $\mu' \simeq \mu$ for p_{lab} in the GeV region. For Class-I reactions, however, μ' is greater than μ at finite energies. For these reactions μ' decreases with increasing energy. The exponential factor $\exp(-\mu' b)/(\mu' b)^{1/2}$ in (8), therefore, increases with increasing energy; the larger the value of b, the larger the increase. Since the large-b partial waves increase in magnitude relative to the small-b partial waves, LRPE decreases with increasing energy more slowly at fixed t' than the Born approximation. For $\mu' \gg \mu$, the difference in energy dependence can be significant at small $-t'$. In Appendix C we give analytic expressions which approximate the LRPE contribution to scattering amplitudes. These expressions give numerical estimates for the magnitude of these energy-dependent effects.

To illustrate the energy dependence of the long-range pion contribution in a particular reaction, we consider $\pi^+ p \to f^0 \Delta^{++}$ between 8 and 16 GeV/c. In this interval, μ'^2 decreases from $6\mu^2$ to $3\mu^2$. In the Born approximation, the differential cross section at $t'=0$ decreases from 12.0 mb (GeV/c)$^{-2}$ at 8 GeV/c to 6.64 mb (GeV/c)$^{-2}$ at 16 GeV/c. The long-range pion contribution to the differential cross section at $t'=0$ decreases more slowly. An estimate of this contribution is obtained by considering the partial-wave amplitudes of the simple Born

[22] See, e.g., J. D. Jackson and G. E. Hite, Phys. Rev. **169**, 1248 (1968); P. H. Frampton, Nucl. Phys. **B7**, 507 (1968).

approximation (6) for $b\geq 7$ $(\mathrm{GeV}/c)^{-1}$ only. These partial waves contribute 1.8 mb $(\mathrm{GeV}/c)^{-2}$ at 8 GeV/c and 1.73 mb $(\mathrm{GeV}/c)^{-2}$ at 16 GeV/c; that is, the long-range pion contribution at $t'=0$ is roughly constant in this energy interval. It is not possible to give the effect of LRPE on the differential cross section at 16 GeV/c without knowing the phases and magnitudes of the partial waves with $b<7$ $(\mathrm{GeV}/c)^{-1}$. The coherent-droplet model does not give the energy dependence of either the droplet or interference parameters. We discuss the effect of LRPE at 16 GeV/c under various assumptions about the droplet and interference parameters. We consider only interference effects in zero-helicity-flip amplitudes because the long-range pion contribution to helicity-flip amplitudes is not important. We consider only helicity-flip-zero and -one droplet amplitudes because only these contribute significantly for $-t'<0.1$ $(\mathrm{GeV}/c)^2$.

If we assume that at 16 GeV/c there is no interference between LRPE and the small-b partial waves, LRPE produces a spike with a magnitude of 1.8 mb $(\mathrm{GeV}/c)^{-2}$. This spike is similar in shape to the spike seen in $\pi^+p\to\rho^0\Delta^{++}$ at 8 GeV/c. It rises above the slowly varying low-partial-wave contributions whose magnitude is not given by our model.

If we assume constructive interference between LRPE and the small-b partial waves at 16 GeV/c, the spike is larger and broader than in the absence of interference. Similarly, if we assume a small amount of destructive interference, the spike is smaller and narrower than in the absence of interference. If we assume large destructive interference, the structure at small $-t'$ depends on the values of the droplet parameters. If, for example, the droplet parameters are such that in the absence of interference the small-b partial-wave contributions at $t'=0$ are greater than or comparable to the long-range pion contributions, then complete destructive interference in zero-helicity-flip amplitudes would give a dip in the forward direction.

To summarize, LRPE produces a spike in $\pi^+p\to f^0\Delta^{++}$ at 16 GeV/c for most assumptions about the energy dependence of the droplet and interference parameters. The shape and magnitude of the differential cross section for $-t'<\mu'^2$ depends sensitively on interference between LRPE and the small-b partial waves in zero-helicity-flip amplitudes. A measurement of the differential cross section in the region would give information about the phases of the small-b partial waves with helicity flip zero.

ACKNOWLEDGMENTS

It is a pleasure to thank Professor Nina Byers for suggesting the problem and for her help and encouragement. I would also like to thank Professor Sir Rudolph Peierls for his kind hospitality at Oxford University where this work was begun.

APPENDIX A

In this appendix we consider the helicity vertex functions for the vertex $ca\pi$ when the mass, spin, and parity of particles c and a are arbitrary.

The pion helicity vertex function can be written in terms of the collinear matrix element as follows[23]:

$$\langle p_c,\theta,\lambda_c;s_c\,|\,j_\pi(0)\,|\,p_a,0,\lambda_a;s_a\rangle = \sum_{\mu,\mu'} d_{\mu\lambda_c}^{s_c}(\omega)\,d_{\mu'\lambda_a}^{s_a}(-\theta') \times\langle p_c',0,\mu;s_c\,|\,j_\pi(0)\,|\,0,0,\mu';s_a\rangle, \quad (A1)$$

where[23]

$$p_c'=\{[-t+(m_c-m_a)^2][-t+(m_c+m_a)^2]/4m_a^2\}^{1/2}, \quad (A2)$$

$$p_c'\cos\omega=(p_cE_a-p_aE_c\cos\theta)/m_a, \quad (A3)$$

$$p_c'\sin\omega=-(m_c/m_a)\,p_a\sin\theta, \quad (A4)$$

$$p_c'\cos\theta'=-(p_aE_c-p_cE_a\cos\theta)/m_a, \quad (A5)$$

$$p_c'\sin\theta'=p_c\sin\theta. \quad (A6)$$

The collinear matrix element can be expanded using the Wigner-Eckart theorem[24,25]:

$$\langle p_c',0,\mu;s_c\,|\,j_\pi(0)\,|\,0,0,\mu';s_a\rangle = \sum_L C(s_c,L,s_a;\mu,0,\mu')\,T^{s_cs_a}{}_L(t,m_c,m_a). \quad (A7)$$

Here L is the relative orbital angular momentum of the pion and particle c.

Parity conservation imposes the following restriction on L:

$$(-1)^L=-\eta_c\eta_a, \quad (A8)$$

where η_c and η_a are the intrinsic parities of particles c and a.

From nonrelativistic quantum mechanics, which is valid near $p_c'=0$, one finds that as $p_c'\to 0$ the reduced matrix elements $T^{s_cs_a}{}_L(t,m_c,m_a)$ vanish at least as fast as $(p_c')^L$. Since p_c' vanishes like $[t-(m_c-m_a)]^{1/2}$, one can write

$$T^{s_cs_a}{}_L(t,m_c,m_a)=[t-(m_c-m_a)^2]^{L/2}f^{s_cs_a}{}_L(t,m_c,m_a), \quad (A9)$$

where $f^{s_cs_a}{}_L$ is finite at $t=(m_c-m_a)^2$. Similar considerations for the decay of a pion with mass $\sqrt{t}$ into particle a and the antiparticle of c show that near $t=(m_c+m_a)^2$,

$$f^{s_cs_a}{}_L(t,m_c,m_a)\propto[t-(m_c+m_a)^2]^{L'/2}, \quad (A10)$$

where L' is the minimum allowed relative angular momentum of a and the antiparticle of c. For a and c bosons, $L'=L$; for fermions, L' is either $L+1$ or $L-1$.

[23] G. C. Wick, Ann. Phys. (N.Y.) **18**, 65 (1962).
[24] M. E. Rose, *Elementary Theory of Angular Momentum* (Wiley, New York, 1957).
[25] L. Durand, III, P. C. DeCelles, and R. B. Marr, Phys. Rev. **126**, 1882 (1962).

The behavior of the helicity vertex functions near $t=(m_c+m_a)^2$ is not important in determining the behavior of the long-range pion contribution to the differential cross section near $t=0$. We, therefore, do not make explicit the behavior (A10) in succeeding formulas.

Using (A7) and (A9), we rewrite (A1) in such a way that the behavior of the helicity vertex functions for small t can be determined easily:

$$\langle p_c, \theta, \lambda_c; s_c \mid j_\pi(0) \mid p_a, 0, \lambda_a; s_a\rangle = \sum_{L,\mu} d_{\mu\lambda_c}^{s_c}(\omega)\, d_{\mu\lambda_a}^{s_a}(-\theta')\, C(s_c, L, s_a; \mu, 0, \mu) \times[-t+(m_c-m_a)^2]^{L/2} f^{s_c s_a}{}_L(t, m_c, m_a). \quad \text{(A11)}$$

We see immediately that all helicity vertex functions with $m_c=m_a$ vanish as $t\to 0$ at least as fast as $(-t)^{L/2}$, where $L\geq \mid s_c-s_a\mid$ and $(-1)^L=-\eta_c\eta_a$.

For all scattering reactions with pion exchange for which there are data at present, the spin parity of one of the particles, either c or a, is either 0^- or $\frac{1}{2}^+$. If we take $s_a{}^{\eta_a}$ to be either 0^- or $\frac{1}{2}^+$, the sum over L in (A11) includes only one term due to the restrictions (A7) and (A8).

When only one value of L is allowed, the helicity vertex function can be written

$$\langle p_c, \theta, \lambda_c; s_c \mid j_\pi(0) \mid p_a, 0, \lambda_a; s_a\rangle = W_{\lambda_c\lambda_a}{}^{s_c s_a L}(\omega, \theta')\, T^{s_c s_a}{}_L(t, m_c, m_a), \quad \text{(A12)}$$

where $T^{s_c s_a}{}_L$ is defined in (A12) and

$$W_{\lambda_c\lambda_a}{}^{s_c s_a L}(\omega, \theta') = \sum_{\mu} d_{\mu\lambda_c}^{s_c}(\omega)\, d_{\mu\lambda_a}^{s_a}(-\theta') \times C(s_c, L, s_a; \mu, 0, \mu). \quad \text{(A13)}$$

The relative magnitudes of helicity vertex functions with different (λ_c, λ_a) depend only on $W_{\lambda_c\lambda_a}{}^{s_c s_a L}(\omega, \theta')$ and not on $T^{s_c s_a}{}_L$. For $s_a=0$, the sum over μ in (A13) contains only $\mu=0$; for $s_a=\frac{1}{2}$, the sum contains only $\mu=\pm\frac{1}{2}$.

For $m_c\neq m_a$, ω and θ' are proportional to θ as $\theta\to 0$. Thus, as $\theta\to 0$,

$$W_{\lambda_c\lambda_a}{}^{s_c s_a L}(\omega, \theta') \propto (\sqrt{-t'})^{\mid\lambda_c-\lambda_a\mid}. \quad \text{(A14)}$$

Unless $f^{s_c s_a}{}_L$ vanishes at $t'=0$, for $m_c\neq m_a$ all the helicity vertex functions vanish like the minimum power of $\sqrt{(-t')}$ required to conserve angular momentum. This behavior has the consequence that for $-t'$ sufficiently small, the largest helicity vertex functions are those with the smallest amount of helicity flip.

For $m_c=m_a$ and $\mid \mathbf{p}_c\mid = \mid \mathbf{p}_a\mid$, ω and θ' are not proportional to θ for small θ, in contrast to the unequal-mass case. Under these conditions, $\theta'=\pi+\omega$ and $\theta=\theta'+\omega$. As $\theta\to 0$, $\omega\to -\frac{1}{2}\pi$ and $\theta'\to\frac{1}{2}\pi$. As a result of the different behavior of ω and θ', the relative magnitudes of the helicity vertex functions at small t' are different in the equal-mass case from the relative magnitudes in the unequal-mass case.

We consider first the most important equal-mass vertex, the nucleon-nucleon vertex. For $m_c=m_a$ and $\mid \mathbf{p}_c\mid = \mid \mathbf{p}_a\mid$, then $\theta'=\pi+\omega$. For $\lambda_c=\lambda_a\equiv\lambda$, we find

$$W_{\lambda\lambda}{}^{\frac{1}{2}\frac{1}{2}1}(\omega, \pi+\omega)=0. \quad \text{(A15)}$$

For $\lambda_c=-\lambda_a\equiv\lambda$, we find

$$W_{\lambda-\lambda}{}^{\frac{1}{2}\frac{1}{2}1}(\omega, \pi+\omega)=1/\sqrt{3}. \quad \text{(A16)}$$

Thus for $\mid \mathbf{p}_c\mid = \mid \mathbf{p}_a\mid$, the nucleon-pion vertex function vanishes for all t when $\lambda_c-\lambda_a=0$. When $\mid \lambda_c-\lambda_a\mid =1$, it vanishes like $\sqrt{(-t)}$.

Next we determine the relative magnitudes of helicity vertex functions near $t=0$ for the equal-mass case when the parities of c and a and the spin of c are arbitrary and $s_a=0$ or $\frac{1}{2}$. At $t=0$, for $m_c=m_a$, $\omega=-\frac{1}{2}\pi$ and $\theta'=\frac{1}{2}\pi$. We consider first $s_a=\frac{1}{2}$. Then at $t=0$, $W_{\lambda_c\lambda_a}{}^{s_c\frac{1}{2}L}(\omega, \theta')$ becomes

$$W_{\lambda_c\lambda_a}{}^{s_c\frac{1}{2}L}(-\tfrac{1}{2}\pi, \tfrac{1}{2}\pi) = \sum_{\mu=\pm\frac{1}{2}} d_{\mu\lambda_c}^{s_c}(-\tfrac{1}{2}\pi)\, d_{\mu\lambda_a}^{\frac{1}{2}}(-\tfrac{1}{2}\pi) \times C(s_c, L, \tfrac{1}{2}; \mu, 0, \mu). \quad \text{(A17)}$$

Using[24]

$$C(j_1, j_2, j_3; m_1, m_2, m_3) = (-1)^{j_1+j_2-j_3} \times C(j_1, j_2, j_3; -m_1, -m_2, -m_3) \quad \text{(A18)}$$

and[14]

$$d_{\lambda\mu}^{j}(-\tfrac{1}{2}\pi) = (-1)^{j+\mu} d_{-\lambda\mu}^{j}(-\tfrac{1}{2}\pi), \quad \text{(A19)}$$

we rewrite (A17) in the following form:

$$W_{\lambda_c\lambda_a}{}^{s_c\frac{1}{2}L}(-\tfrac{1}{2}\pi, \tfrac{1}{2}\pi) = C(s_c, L, \tfrac{1}{2}; \tfrac{1}{2}, 0, \tfrac{1}{2}) \times[1-\eta_c\eta_a(-1)^{\lambda_c-\lambda_a}]\, d_{\frac{1}{2}\lambda_c}^{s_c}(-\tfrac{1}{2}\pi)\, d_{\frac{1}{2}\lambda_a}^{\frac{1}{2}}(-\tfrac{1}{2}\pi), \quad \text{(A20)}$$

where we have also used (A8). Thus we find

$$W_{\lambda_c\lambda_a}{}^{s_c\frac{1}{2}L}(-\tfrac{1}{2}\pi, \tfrac{1}{2}\pi)=0 \quad \text{(A21)}$$

if

$$\eta_a\eta_c(-1)^{\lambda_a-\lambda_c}=1. \quad \text{(A22)}$$

However, we find

$$W_{\lambda_c\lambda_a}{}^{s_c\frac{1}{2}L}(-\tfrac{1}{2}\pi, \tfrac{1}{2}\pi)\neq 0 \quad \text{(A23)}$$

if

$$\eta_a\eta_c(-1)^{\lambda_a-\lambda_c}=-1. \quad \text{(A24)}$$

Therefore, for equal-mass pion vertices with $s_a=\frac{1}{2}$, for small t and $\eta_a=\eta_c$, helicity vertex functions with $\mid \lambda_a-\lambda_c\mid =$(even) are smaller in magnitude than the helicity vertex functions with $\mid \lambda_a-\lambda_c\mid =$(odd). The well-known behavior of the nucleon-pion vertex function is a special case of this result. For the same conditions on the masses, spins, and t, but with $\eta_a=-\eta_c$, helicity vertex functions with $\mid \lambda_a-\lambda_c\mid =$(odd) are smaller in magnitude than the helicity vertex functions with $\mid \lambda_a-\lambda_c\mid =$(even).

The results of the previous paragraph for $s_a=\frac{1}{2}$ hold also for $s_a=0$. For $s_a=0$, there is an additional result, namely, the pion helicity vertex function vanishes for all t unless

$$(-1)^{s_c}=-\eta_a\eta_c. \quad \text{(A25)}$$

These results can be proved simply using (A13) and known properties of $d_{0\lambda}^{s}(\frac{1}{2}\pi)$.

APPENDIX B

In this appendix we give detailed expressions for the pion helicity vertex functions for the reactions we considered in this paper. The vertex functions are calculated in perturbation theory. Perturbation theory gives the most general helicity dependence of the vertex functions.

Our notation is as follows: $P_c=(E_c, p_c\sin\theta, 0, p_c\cos\theta)$, $P_a=(E_a, 0, 0, p_a)$, and $P_\mu P^\mu=m^2$. The momentum transfer is $t=(P_a-P_c)^2$. We denote the spin-1 polarization vector by e_μ and the spinor for spin $\frac{1}{2}$ by u. The spinor u is normalized by

$$\bar{u}(\lambda, P)u(\lambda, P)=1. \tag{B1}$$

The spinor for spin $\frac{3}{2}$ was constructed using

$$u_\mu(\lambda, P)=\sum_{\lambda'} C(1, \tfrac{1}{2}, \tfrac{3}{2}; \lambda', \lambda-\lambda', \lambda)e_\mu(\lambda', P)u(\lambda-\lambda', P). \tag{B2}$$

Similarly, the spin-2 polarization tensor $e_{\mu\nu}$ was constructed as follows:

$$e_{\mu\nu}(\lambda, P)=\sum_{\lambda'} C(1, 1, 2; \lambda', \lambda-\lambda', \lambda) \times e_\mu(\lambda', P)e_\nu(\lambda-\lambda', P). \tag{B3}$$

Note that the single-particle helicity states in this appendix are type-"1" states in the notation of Jacob and Wick.[14] In constructing scattering amplitudes one must use type-"1" states at one vertex and type-"2" states at the other. The vertex functions for type-"2" particles differ by a factor $(-1)^{s_c-\lambda_c+s_a-\lambda_a}$ from those for type-"1" particles. These phase factors are important in determining the absolute phases of the partial-wave amplitudes and in calculating density-matrix elements.

Vertex: $1^-0^-0^-$; coupling mode: $e_\mu(P_c, \lambda_c)P_a^\mu$.

$$e_\mu(P_c, \pm1)P_a^\mu=\mp(p_a\sin\theta)/\sqrt{2}, \tag{B4}$$

$$e_\mu(P_c, 0)P_a^\mu=(p_cE_a-p_aE_c\cos\theta)/m_c. \tag{B5}$$

Vertex: $2^+0^-0^-$; coupling mode: $e_{\mu\nu}(P_c, \lambda_c)P_a^\mu P_a^\nu$.

$$e_{\mu\nu}(P_c, \pm2)P_a^\mu P_a^\nu=\tfrac{1}{2}p_a^2\sin^2\theta, \tag{B6}$$

$$e_{\mu\nu}(P_c, \pm1)P_a^\mu P_a^\nu=\mp(p_cE_a-p_aE_c\cos\theta)p_a\sin\theta/m_c, \tag{B7}$$

$$e_{\mu\nu}(P_c, 0)P_a^\mu P_a^\nu=(\sqrt{\tfrac{2}{3}})(p_cE_a-p_aE_c\cos\theta)^2/m_c^2 - (\sqrt{\tfrac{1}{6}})p_a^2\sin^2\theta. \tag{B8}$$

Vertex: $\frac{1}{2}^+\frac{1}{2}^+0^-$; coupling mode: $\bar{u}(P_c, \lambda_c)\gamma_5 u(P_a, \lambda_a)$.

$$\bar{u}(P_c, \tfrac{1}{2})\gamma_5 u(P_a, \tfrac{1}{2})=\eta_-\cos\tfrac{1}{2}\theta, \tag{B9}$$

$$\bar{u}(P_c, -\tfrac{1}{2})\gamma_5 u(P_a, \tfrac{1}{2})=-\eta_+\sin\tfrac{1}{2}\theta, \tag{B10}$$

$$\bar{u}(P_c, \tfrac{1}{2})\gamma_5 u(P_a, -\tfrac{1}{2})=-\eta_+\sin\tfrac{1}{2}\theta, \tag{B11}$$

$$\bar{u}(P_c, -\tfrac{1}{2})\gamma_5 u(P_a, -\tfrac{1}{2})=-\eta_-\cos\tfrac{1}{2}\theta. \tag{B12}$$

In these expressions $\eta_\pm$ is given by

$$\eta_\pm=\left[\frac{(E_c+m_c)(E_a+m_a)}{4m_am_c}\right]^{1/2}\left[\frac{p_a}{E_a+m_a}\pm\frac{p_c}{E_c+m_c}\right]. \tag{B13}$$

Vertex: $\frac{3}{2}^+\frac{1}{2}^+0^-$; coupling mode: $\bar{u}_\mu(P_c, \lambda_c)P_a^\mu u(P_a, \lambda_a)$.

$$\bar{u}_\mu(P_c, \tfrac{3}{2})P_a^\mu u(P_a, \tfrac{1}{2})=-\eta_-'(p_a\sin\theta/\sqrt{2})\cos\tfrac{1}{2}\theta, \tag{B14}$$

$$\bar{u}_\mu(P_c, \tfrac{3}{2})P_a^\mu u(P_a, -\tfrac{1}{2})=-\eta_+'(p_a\sin\theta/\sqrt{2})\sin\tfrac{1}{2}\theta, \tag{B15}$$

$$\bar{u}_\mu(P_c, \tfrac{1}{2})P_a^\mu u(P_a, \tfrac{1}{2})=(\sqrt{\tfrac{2}{3}})\eta_-'[(p_cE_a-p_aE_c\cos\theta)/m_c] \times\cos\tfrac{1}{2}\theta+\eta_+'(p_a\sin\theta/\sqrt{6})\sin\tfrac{1}{2}\theta, \tag{B16}$$

$$\bar{u}_\mu(P_c, \tfrac{1}{2})P_a^\mu u(P_a, -\tfrac{1}{2})=(\sqrt{\tfrac{2}{3}})\eta_+'[(p_cE_a-p_aE_c\cos\theta)/m_c] \times\sin\tfrac{1}{2}\theta-\eta_-'(p_a\sin\theta/\sqrt{6})\cos\tfrac{1}{2}\theta. \tag{B17}$$

In these expressions $\eta_\pm'$ is given by

$$\eta_\pm'=\frac{1}{2}\frac{(E_c+m_c)(E_a+m_a)\pm p_ap_c}{[(E_c+m_c)(E_a+m_a)m_cm_a]^{1/2}}. \tag{B18}$$

The parity-conservation constraint,

$$\bar{u}_\mu(P_c, \lambda_c)P_a^\mu u(P_a, \lambda_a)=(-1)^{\lambda_c-\lambda_a}\bar{u}_\mu(P_c, -\lambda_c) \times P_a^\mu u(P_a, -\lambda_a), \tag{B19}$$

can be used to determine all the other $\bar{u}_\mu P_a^\mu u$ for the vertex $\frac{3}{2}^+\frac{1}{2}^+0^-$.

APPENDIX C

In this appendix we introduce an interpolation of LRPE to small b which yields expressions for scattering amplitudes which are particularly simple. These expressions give convenient numerical estimates of the long-range pion contribution to scattering amplitudes. We introduce the interpolation

$$\alpha_{\{\lambda\}}{}'^{\pi}=R_{\{\lambda\}}{}^{\pi}(b^2/(b^2+a_{|\Delta\lambda|}{}^2))^{|\Delta\lambda|/2} \times K_{\Delta\lambda}(\mu'(b^2+a_{|\Delta\lambda|}{}^2)^{1/2}), \tag{C1}$$

where $a_{|\Delta\lambda|}$ is a parameter. Varying $a_{|\Delta\lambda|}$ gives a family of different interpolations of LRPE to small b. For this family of interpolations, $f_{\Delta\lambda}{}'^{\pi}$ is given by

$$f_{\Delta\lambda}{}'^{\pi}(s, t')=\int b\,db\,J_{\Delta\lambda}(b\sqrt{-t'})[b^2/(b^2+a_{|\Delta\lambda|}{}^2)]^{|\Delta\lambda|/2} \times K_{\Delta\lambda}(\mu'(b^2+a_{|\Delta\lambda|}{}^2)^{1/2}). \tag{C2}$$

Integrating, we find[26]

$$f_{\Delta\lambda}{}'^{\pi}(s, t')=(-1)^{(\Delta\lambda-|\Delta\lambda|)/2}(-t'/\mu'^2)^{|\Delta\lambda|/2} \times[a_{|\Delta\lambda|}/(\mu^2-t)^{1/2}]K_1(a_{|\Delta\lambda|}(\mu^2-t)^{1/2}). \tag{C3}$$

We see immediately from Eq. (C3) that $f_{\Delta\lambda}{}'^{\pi}$ has a pole at $t=\mu^2$ with residue $-(-1)^{\Delta\lambda/2}$. The position and residue of the pole are independent of $a_{|\Delta\lambda|}$. The value of $f_{\Delta\lambda}{}'^{\pi}$ away from $t=\mu^2$ does depend on $a_{|\Delta\lambda|}$, that is,

[26] G. N. Watson, *Theory of Bessel Functions* (Cambridge U. P., Cambridge, 1966), p. 416.

it depends on the way in which LRPE is interpolated to small b. Since there is no unique way to make this interpolation, we must make an arbitrary choice. In our calculations we used the interpolation Eq. (22). Here we show how $f_{\Delta\lambda}{}'^{\pi}$ can be used to approximate $f_{\Delta\lambda}{}^{\pi}$ [see Eq. (27)].

The functions $f_{\Delta\lambda}{}^{\pi}$ depend on the two elastic scattering parameters c and a. For meson-baryon scattering $c=0.58$ and $a=4.5$. We can effectively take into account the absorption appropriate to meson-baryon scattering contained in $f_{\Delta\lambda}{}^{\pi}$ by choosing $a_0=5.25$ $(\mathrm{GeV}/c)^{-1}$ and $a_1=6.2$ $(\mathrm{GeV}/c)^{-1}$ in $f_{\Delta\lambda}{}'^{\pi}$. For $\Delta\lambda=0$ and $\mu'=\mu$, the equality $f_0{}^{\pi}=f_0{}'^{\pi}$ is valid to 5% for $-t\leq\mu^2$. For $\mu'=1.5\mu$, the equality $f_0{}^{\pi}=f_0{}'^{\pi}$ is valid to 10% for $-t'\leq\mu'^2$. For $\Delta\lambda=1$ and $\mu'=\mu$, the equality $f_1{}^{\pi}=f_1{}'^{\pi}$ is valid to 10% for $-t\leq 2\mu^2$. For $\mu'=1.5\mu$, the equality $f_1{}^{\pi}=f_1{}'^{\pi}$ is valid to 15% for $-t'\leq 2\mu'^2$. For baryon-baryon scattering the absorption in $f_{\Delta\lambda}{}^{\pi}$ is larger. For this case, for $\Delta\lambda=0$ and $\Delta\lambda=1$ and $\mu'=\mu$, $f_{\Delta\lambda}{}^{\pi}=f_{\Delta\lambda}{}'^{\pi}$ within 15% for $-t\leq\mu^2$ when $a_0=6.25$ $(\mathrm{GeV}/c)^{-1}$ and $a_1=6.75$ $(\mathrm{GeV}/c)^{-1}$.

Note that Eq. (C3) gives the energy dependence of LRPE at $t'=0$ to be

$$f_0{}'^{\pi}(s,t'=0)=(-1)^{(\Delta\lambda-|\Delta\lambda|)/2}(a_0/\mu')K_1(a_0\mu'). \quad \text{(C4)}$$

For a_0 nonzero and energy independent, $f_0{}'^{\pi}(s,t'=0)$ decreases with energy more slowly than the Born approximation, which is given by the limit $a_0=0$.

PHYSICAL REVIEW D VOLUME 1, NUMBER 9 1 MAY 1970

Pion-Pion Scattering Information from $e^-e^+\to\pi^-\pi^+\gamma$†

M. J. Creutz* and M. B. Einhorn
Stanford Linear Accelerator Center, Stanford University, Stanford, California 94305

(Received 29 December 1969)

We show how the reaction $e^-e^+\to\pi^-\pi^+\gamma$ can be used to study the dipion system in states of even charge conjugation (and even angular momentum). In particular, its utility for experimentally investigating an $I=0$, $J=0$ resonance (ϵ meson) is discussed in detail.

INTRODUCTION

To lowest order in the fine-structure constant α, the reaction $e^-+e^+\to H$ (H being any neutral hadronic system) produces only final states with charge conjugation (C) odd and angular momentum (J) equal to unity. This property is one of the primary advantages of electron-positron colliding beam experiments; i.e., it allows the careful experimental study of a specific hadronic channel. Already this reaction has yielded beautiful results on the pion[1] and kaon[2] form factors as well as the three-pion final state.[2,3] However, this property is at the same time one of the limitations of electron-positron storage rings, since one would also like to investigate experimentally other hadronic channels. In a previous paper,[4] we showed how one could use reactions of the form

$$e^-+e^+\to H+\gamma,$$

where γ is a hard photon, to study hadronic systems with even C. Although the hadrons H may emerge from this reaction with either even or odd C, quantum electrodynamics plus knowledge of the cross section for $e^-+e^+\to H$ allows one to remove the odd-C contribution. Consequently, the effects of the production of hadronic states with even C can be isolated and studied in a model-independent way. We have illustrated[4] the method of analysis by considering the reaction

$$e^-+e^+\to\pi^-+\pi^++\gamma.$$

In this expanded discussion we will present the details of the analysis and consider further experimental problems and theoretical implications.

The outline of the paper is as follows: In Sec. I we summarize the theoretical predictions and experimental results bearing on the existence of an $I=0$, $J=0$ dipion resonance (the ϵ meson). In Sec. II we discuss the kinematics of the reaction being considered. We include here a brief discussion of how such an experiment may be analyzed and discuss some features of the Dalitz plot. In Sec. III a particular model for estimating the order of magnitude of the contribution from the ϵ meson is presented. In Sec. IV we discuss the constraints that unitarity imposes on the production amplitude. We point out in particular that there is no simple analog here of the Fermi-Watson final-state

† Work supported by the U.S. Atomic Energy Commission.
* NSF Graduate Fellow.
[1] J. E. Augustin *et al.*, Phys. Letters **28B**, 508 (1969); V. L. Auslander *et al.*, *ibid.* **25B**, 433 (1967).
[2] J. E. Augustin *et al.*, Phys. Letters **28B**, 517 (1969).
[3] J. E. Augustin *et al.*, Phys. Letters **28B**, 513 (1969).
[4] M. J. Creutz and M. B. Einhorn, Phys. Rev. Letters **24**, 341 (1970) (hereafter referred to as L).